Remarks on the Geometry of High Energy Nuclear Collisions

Peter Jacobs (LBNL) and Glenn Cooper (UCB/LBNL)

STAR Note 402
Submitted June 24, 1999; Revised January 4, 2000*

Abstract

We discuss several aspects of the geometry of nuclear collisions relevant to STAR and RHIC, within the framework of the familiar Glauber formalism. An analytical rule is derived for the scaling of hard process rates with system size in the absence of nuclear effects, and baseline predictions are made for single inclusive pion rates at high $\mathrm{p}_\perp$. The initial shape of the interaction region for noncentral collisions is discussed for several simple interaction models, and moments of these distributions projected into the transverse plane are calculated. The number of nucleon participants and binary collisions for these models is also calculated. The radial distribution of hard scatterings relative to the center of the colliding nuclei is presented.

1 Introduction

The distributions of many observables measured in high energy nuclear collisions are dominated by simple effects of nuclear geometry. Familiar examples are $d\sigma/d\mathrm{E}_\perp$ and $d\sigma/d\mathrm{M}$, where $\mathrm{E}_\perp$ is the transverse energy and M is the multiplicity measured in a large rapidity interval. The search for new phenomena at RHIC will require the comparison of distributions of observables from colliding systems of varying initial size and shape, achieved experimentally through variation of the mass of the beams and the centrality of the collision[1]. New phenomena may be identifiable by deviations of distributions from conventional, hadronic scenarios, but they must be distinguished from the simple geometric effects. Understanding the influence of nuclear geometry on each observable is thus an important ingredient to understanding RHIC data.

At energies at which nuclear collisions have been studied until now ($\sqrt{s_{\mathrm{NN}}} \leq 20\ \mathrm{GeV}$), the distributions of coarse quantities such as $\mathrm{E}_\perp$ or M in a large rapidity interval scale with the estimated number of excited nucleons, the so-called Wounded

*Revisions are: correction to the exponent of A in eqn. (14) and following text, and correction of some numerical errors in Tables 1 and 2.

[1]We will not discuss the important experimental questions associated with estimating "centrality" or impact parameter of a collision.

Nucleon scaling first observed in proton-nucleus collisions [1, 2]. A new ingredient in this discussion emerges when considering nuclear collisions at RHIC energies and beyond: at RHIC, hard processes contribute significantly (of order 50% [3]) to $\mathrm{E}_\perp$ and M. The number of hard scatterings in an event is expected to scale roughly with the number of binary nucleon-nucleon collisions, not the number of excited nucleons, so that the relationship between geometry of the collision and $d\sigma/d\mathrm{E}_\perp$ or $d\sigma/d\mathrm{M}$ will be different at RHIC than at lower energies.

In this note, we discuss several aspects of the geometry of nuclear collisions relevant to STAR and RHIC. Nuclear geometry and its connection to experimental observables in high energy collisions has been discussed for many years, dating back at least to Glauber [4]. It would be surprising if there is anything new to say about it, and there is indeed nothing basically new in this note. We apply a simple, widely used formalism [3, 5] and plot distributions that give some insight into geometrical effects in nuclear collisions. These distributions are intrinsic to calculations utilizing this formalism, but previous authors (that we have found) simply have not plotted them explicitly. In addition, we derive a scaling rule for the dependence of the rate of hard processes on system mass, and apply it to observables relevant to STAR Year 1.

We present the formalism in section 2. Section 3 discusses the scaling of the rate of hard processes (small cross sections) with system mass, section 4 discusses the transverse profile of the interaction volume for non-central collisions, section 5 presents the number of nucleon participants and binary collisions per nuclear collision, and section 6 discusses the radial distribution of hard processes relative to the center of one of the colliding nuclei.

2 Formalism

The coordinate system is defined in Figure 1. We utilize the standard nuclear thickness function $\mathrm{T_A}$ [5],

$$\mathrm{T_A}(|\vec{s}|) = \int dz \rho_\mathrm{A}(z, \vec{s}). \tag{1}$$

For the nuclear density we use a Woods-Saxon distribution,

$$\rho_\mathrm{A}(r) = \rho_0 \cdot \frac{1}{1 + e^{(r-\mathrm{R_A})/\mathrm{a}}}, \tag{2}$$

where $r = \sqrt{s^2 + z^2}$, $\mathrm{R_A} = 1.12 \cdot \mathrm{A}^{1/3}$, and $\rho_0 = 0.159$ GeV/fm^3 and a=0.535 fm for ^{197}Au. ρ_A is normalized so that $\int d^2s \mathrm{T_A}(|\vec{s}|) = \mathrm{A}$.

In Fig. 1, the nuclear impact parameter is denoted b, and the distance to a point in the transverse plane from the center of either nucleus is denoted $\mathrm{b_A}$ and $\mathrm{b_B}$. The vector from the origin to this point is written

$$\vec{s} = \vec{\mathrm{b_A}} - \frac{b}{2}\hat{x} = \vec{\mathrm{b_B}} + \frac{b}{2}\hat{x}. \tag{3}$$

where $\hat{x}$ is the unit vector in the x direction.

We now consider some scaling rules of rates and cross sections relative to nucleon-nucleon collisions for nuclear collisions at a given nuclear impact parameter:

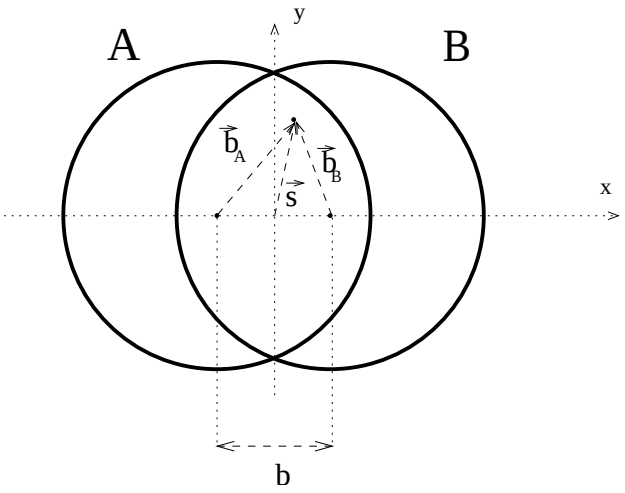

Figure 1: Transverse coordinate system. A and B are the masses of the colliding nuclei. The incoming beams are (anti-)parallel to the z axis. The x-z plane is commonly called the reaction plane.

- Wounded Nucleon Scaling: We consider the number of nucleons at $\vec{s}$ that are struck at least once by the nucleons in the oncoming nucleus, where "struck" means inelastically excited with nucleon-nucleon collision cross section[2] $\sigma_{\rm NN}$. In the transverse projection, the density of wounded nucleons per nuclear collision is given in units $1/\mathrm{fm}^2$ by:

$$\frac{\mathrm{d}^2\mathrm{N_{WN}}}{\mathrm{ds}^2} = \mathrm{T_A(b_A)}\cdot(1-e^{-\mathrm{T_B(b_B)}\sigma_{\rm NN}})+\mathrm{T_B(b_B)}\cdot(1-e^{-\mathrm{T_A(b_A)}\sigma_{\rm NN}}), \quad (4)$$

  where the dependence on nuclear impact parameter is via Eq. 3.

- Binary Collision Scaling: More generally, we mean those processes with sufficiently small nucleon-nucleon cross section $\sigma_{\rm NN}^{\rm hard}$ that $\mathrm{T_A}\cdot\sigma_{\rm NN}^{\rm hard}\ll 1$ (we apply the label "hard" because we are usually refering to high momentum transfer processes, or hard scattering). Nucleon-nucleon interaction probabilities can be added for the total interaction probability, and the number of hard scatterings per nuclear collision goes as the number of binary nucleon-nucleon collisions. The density in the transverse projection of hard processes per nuclear collision, in units $1/\mathrm{fm}^2$, is then

$$\frac{\mathrm{d}^2\mathrm{N_{hard}}}{\mathrm{ds}^2} = \sigma_{\rm NN}^{\rm hard}\cdot\mathrm{T_A(b_A)}\cdot\mathrm{T_B(b_B)}. \quad (5)$$

  Integrating over the transverse plane (and changing integration variables), the total number of hard processes per nuclear collision is given as a function of

[2] $\sigma_{\rm NN}\approx$ 30 mb at the SPS ($\sqrt{s_{\rm NN}}$=20 GeV) and 40 mb at RHIC ($\sqrt{s_{\rm NN}}$=200 GeV).

nuclear impact parameter b by[3, 5]:

$$\mathrm{N_{hard}}(b) = \sigma_{\mathrm{NN}}^{\mathrm{hard}} \cdot \int d^2s \mathrm{T_A}(|\vec{s}|)\mathrm{T_B}(|\vec{b}-\vec{s}|) \equiv \sigma_{\mathrm{NN}}^{\mathrm{hard}} \cdot \mathrm{T_{AB}}(b) \qquad (6)$$

The geometric scaling rule for the mean number of hard processes per nuclear collision, with no restriction on collision geometry, is

$$\begin{aligned} < \mathrm{N_{hard}} > &\equiv \sigma_{\mathrm{AB}}^{\mathrm{hard}}/\sigma_{\mathrm{AB}}^{\mathrm{geom}} & (7)\\ &= (\sigma_{\mathrm{NN}}^{\mathrm{hard}} \int d^2b \mathrm{T_{AB}}(b))/\sigma_{\mathrm{AB}}^{\mathrm{geom}} & (8)\\ &= (AB \cdot \sigma_{\mathrm{NN}}^{\mathrm{hard}})/\sigma_{\mathrm{AB}}^{\mathrm{geom}}, & (9) \end{aligned}$$

where $\sigma_{\mathrm{AB}}^{\mathrm{geom}}$ is the geometric (inelastic) nucleus-nucleus cross section and $\sigma_{\mathrm{AB}}^{\mathrm{hard}}$ is the total cross section in nuclear collisions A+B for the hard process under consideration. Thus, neglecting nuclear effects,

$$\sigma_{\mathrm{AB}}^{\mathrm{hard}} = (\mathrm{AB}) \cdot \sigma_{\mathrm{NN}}^{\mathrm{hard}}. \qquad (10)$$

More generally, nuclear effects will modify this to $\sigma_{\mathrm{AB}}^{\mathrm{hard}} = (\mathrm{AB})^{\alpha} \cdot \sigma_{\mathrm{NN}}^{\mathrm{hard}}$, with α typically less than 1 [6].

3 Rates of Hard Processes

Following reference [5], the fraction of the total cross section for hard processes in nuclear collsions A+B occuring at impact parameters $b < b_c$ is

$$f_{\mathrm{AB}}(b_c) = \frac{2\pi}{\mathrm{AB}} \int_0^{b_c} b db \mathrm{T_{AB}}(b). \qquad (11)$$

The fraction of the geometric cross section with impact parameter $b < b_c$ is

$$f_{\mathrm{geo}}(b_c) = [2\pi \int_0^{b_c} b db (1 - e^{-\mathrm{T_{AB}}\sigma_{\mathrm{NN}}})]/\sigma_{\mathrm{AB}}^{\mathrm{geom}}. \qquad (12)$$

Analogous to equation 9, the number of hard processes per nuclear collision for collisions with impact parameter $b < b_c$ is given by

$$\mathrm{N_{hard}}(b_c) \equiv \frac{\sigma_{\mathrm{AB}}^{\mathrm{hard}}(b < b_c)}{\sigma_{\mathrm{AB}}^{\mathrm{geom}}(b < b_c)} = \frac{\mathrm{AB}\sigma_{\mathrm{NN}}^{\mathrm{hard}}}{\sigma_{\mathrm{AB}}^{\mathrm{geom}}} \frac{f_{\mathrm{AB}}(b_c)}{f_{\mathrm{geo}}(b_c)}. \qquad (13)$$

Figure 2, taken from Ref. [5], shows $f_{\mathrm{AB}}(b_c)$ vs. $f_{\mathrm{geo}}(b_c)$ for symmetric systems of widely varying mass. The striking feature of Fig. 2 is that $f_{\mathrm{AA}}(b_c)/f_{\mathrm{geo}}(b_c)$ is only very weakly dependent upon A, except for the lightest systems. For instance, the most central 10% of the geometric cross section contains 35% of the total hard cross section for Si+Si, 40% for Ag+Ag, and 41% for Au+Au (more extensive tabulation is found in Table 3 of Ref. [5]).

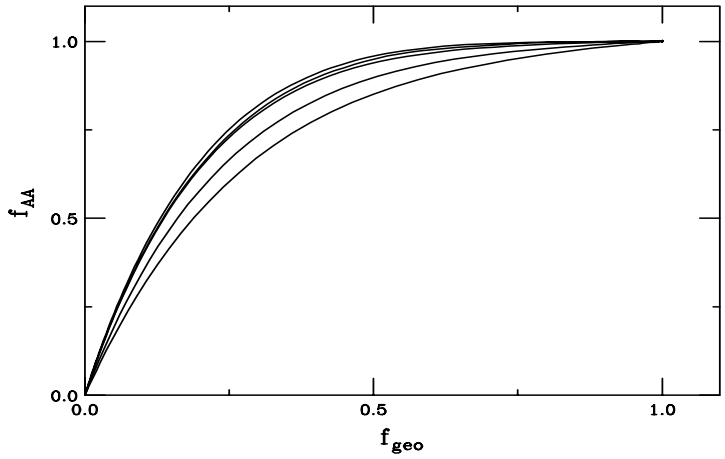

Figure 2: Figure 4 of Ref. [5]: $f_{\rm AA}(b_c)$ (eqn. 11) vs $f_{\rm geo}(b_c)$ (eqn. 12) for symmetric systems A=197, 110, 63, 27 and 16. $f_{\rm AA}(b_c)$ rises most rapidly for the heaviest system.

A significant portion of STAR data will be triggered with a loose cut on centrality ("minimum bias" data). The geometric scaling of hard process rates with system size in this case will follow the appropriate curve in Figure 2.

To determine the A dependence of the number of hard processes per nuclear collision for symmetric systems, we use the geometric cross section $\sigma_{\rm AB}^{\rm geom} \simeq \pi(2{\rm R_A})^2$ with ${\rm R_A} = 1.2{\rm A}^{1/3}$ fm, so that equation 13 becomes

$$ {\rm N_{hard}}(b_c) \simeq 5.5 \cdot 10^{-3} {\rm A}^{4/3} \cdot \frac{\sigma_{\rm NN}^{\rm hard}}{\rm mb} \cdot \frac{f_{\rm AA}(b_c)}{f_{\rm geo}(b_c)}. \qquad (14) $$

Given the insensitivity of $f_{\rm AA}(b_c)/f_{\rm geo}(b_c)$ to A shown in Figure 2, we have the A-dependent geometric scaling rule for hard process rates in the absence of nuclear effects: *for a fixed fraction of the geometric cross section, the number of hard processes (e.g. jets or* ${\rm J}/\Psi$*) per event grows with system size as* $A^{4/3}$. Deviations from this rule indicate nuclear effects such as initial state scattering and shadowing, as well as jet quenching and ${\rm J}/\Psi$ suppression. Because the curves in Fig. 2 are approximately linear at low $f_{\rm geo}(b_c)$, expression 14 is only weakly dependent upon b_c for central collisions. For instance, the mean number of hard processes per nuclear collision is about the same for the 2% and 10% most central collisions (fraction of the total geometric cross section).

Equation 14 can be used to predict the inclusive single particle charged pion and π^0 spectra from different systems, assuming no nuclear effects. We apply it here to scale the existing UA1 data on high ${\rm p}_\perp$ pions from ${\rm p\bar{p}}$ collisions to predict inclusive single particle rates in STAR, for systems under discussion for Year 1 running. The UA1 cross section for single inclusive charged pions is taken from [7]: $d\sigma/dyd{\rm p}_\perp$ = 10^{-3} mb/GeV at ${\rm p}_\perp$=5 GeV and $5 \cdot 10^{-5}$ mb/GeV at ${\rm p}_\perp$=8 GeV. We distinguish two modes of online event selection by STAR:

- Event selection by nuclear collision geometry: Events are selected online on the basis of transverse energy or multiplicity over large acceptance, not by the presence of a high $\mathrm{p}_\perp$ pion. Since high $\mathrm{p}_\perp$ charged pions are measured by the TPC, the $d\sigma/dyd\mathrm{p}_\perp$ given above is scaled up by a factor 2 for two rapidity units of acceptance and a factor 2 for two charge signs. A 50% duty factor is assumed for data taking, giving an overall upward scaling factor of 2 for the rate. Table 1 shows the number of STAR events required for 1000 detected charged pions per GeV bin at 5 and 8 GeV, along with the number of days required for this measurement, for central and minbias Au+Au and Si+Si, and minbias p+p. "Central" is the most central 5% of the geometric cross section. Luminosity is assumed to be high enough that the event rate is limited by the recording bandwidth (20 MB/sec) and assumed event sizes (Au+Au central=20 MB, minbias=1 MB; Si+Si central=3 MB, minimum bias=0.15 MB). The p+p and minimum bias Si+Si recording rates are assumed to be the maximum rate for "empty events", 150 events/second (We are not making precise estimates, so we have not pursued a better gauge of this number with the experts.)

- High $\mathrm{p}_\perp$ π^0 trigger: Events are selected online by means of a high $\mathrm{p}_\perp$ π^0 trigger in the Year 1 EMC acceptance (10% of azimuth, one unit of rapidity). Table 2 shows the event rate per GeV per day of π^0s at 5 and 8 GeV $\mathrm{p}_\perp$ for central and minimum bias Au+Au and Si+Si, and minimum bias p+p, under the stated assumptions for luminosity, and an assumed duty factor for data taking of 50%. "Central" is the most central 5% of the geometric cross section. Event characterization of collision geometry is performed offline, based upon transverse energy or multiplicity in a large acceptance.

Tables 1 and 2 show that high statistics inclusive pion spectra can be measured by STAR well into the perturbative region for a variety of systems in year 1, even if the Si+Si and p+p running periods are restricted to 2-3 weeks each. Nuclear effects due to shadowing are expected to alter these rates on the order of 10-20% [8].

4 Transverse Profile of the Interaction Volume for Non-central Collisions

The azimuthal anisotropy of momentum distributions in nuclear collisions can be related to the orientation of the event plane (the x-z plane in Figure 1) for noncentral collisions over a wide range of energies [9], and has been quantitatively studied up to the highest energy nuclear collisions at the SPS [10]. The lowest order harmonics are referred to as directed and elliptic flow, and are characterized by coefficients v_1 and v_2 respectively in a Fourier expansion of the azimuthal angle or momentum distributions [9].

The azimuthal resolution of the event plane orientation depends upon the magnitude of the flow and the multiplicity of the event. Peripheral collisions of a given system have greater anisotropy but poorer statistical resolution than central events. For a large acceptance experiment at the SPS or RHIC, the highest event plane resolution

System	# evt/day	$p_\perp$ (GeV)	# evt for 1000/GeV	# days
Au+Au central (5%)	$4 \cdot 10^4$	5	$1 \cdot 10^4$	0.24
		8	$2 \cdot 10^5$	5
Au+Au minbias	$8 \cdot 10^5$	5	$4 \cdot 10^4$	0.05
		8	$8 \cdot 10^5$	1
Si+Si central (5%)	$2.5 \cdot 10^5$	5	$1.5 \cdot 10^5$	0.6
		8	$3 \cdot 10^6$	12
Si+Si minbias	$5 \cdot 10^6$	5	$5 \cdot 10^5$	0.1
		8	$1 \cdot 10^7$	2
p+p minbias	$5 \cdot 10^6$	5	$1 \cdot 10^7$	2
		8	$2 \cdot 10^8$	40

Table 1: Online selection of collision geometry: Event sets for high $p_\perp$ charged pions measured in the TPC. Assumptions and details of calculation given in text. Column 4 gives the number of events of a given centrality selection required to obtain 1000 charged pions in a bin of width 1 GeV, centered at a given $p_\perp$.

is expected to be in the neighbourhood of $<\cos(\Psi_{\rm measured} - \Psi_{\rm true})>\approx 0.4$ [9]. With the maturation of techniques to determine the event plane orientation at high energies has come the suggestion to look at the angular dependence of other observables relative to the event plane, such as HBT correlations, jets, and J/Ψ production [9, 11].

Elliptic flow at midrapidity has received particular attention recently because of a possible connection to the Equation of State (see discussion and references in [9]). To help distinguish dynamics from purely geometrical effects, it has been suggested [12, 13] that the measured v_2, the elliptic anisotropy, be scaled by the eccentricity of the reaction volume. This is defined to be [12, 13]

$$\epsilon \equiv \frac{< y^2 > - < x^2 >}{< y^2 > + < x^2 >} \approx \frac{b}{2R_A} \tag{15}$$

where $< \ldots >$ indicates the spatial average over the transverse plane weighted by a density such as that of wounded nucleons (equation 4). The approximation is the ratio of axes of the overlap region in Figure 1, $(y\ |_{x=0})/(x\ |_{y=0})$, not weighted by nuclear density [13].

Given these considerations, we look in some detail at the transverse profile of the reaction volume for noncentral collisions within the geometrical framework outlined in Section 2. This must be done with some caveats in mind, however. We do not incorporate any aspects of longitudinal or transverse dynamics of the nuclear collision, and do not claim to model the collision. These calculations at best indicate the initial geometry of the reaction. However, the formulation of initial conditions in dynamical models such as HIJING and RQMD are similar to Section 2, and the distributions presented here should correspond closely to distributions from those models. Finite formation time of hadrons will smear out the spatial distributions of hard processes presented here, making the observed distributions more isotropic, but we do not attempt to account for this effect.

System	Luminosity $((\mathrm{mb}\cdot\mathrm{sec})^{-1}$)	$\mathrm{p}_\perp$	σ (mb)	#/GeV/day
Au+Au central	0.02	5	0.8	700
		8	0.04	35
Au+Au minbias	0.02	5	4.0	3400
		8	0.2	170
Si+Si central	4.0	5	0.014	2400
		8	$7\cdot10^{-4}$	120
Si+Si minbias	4.0	5	0.078	$1.4\cdot10^{4}$
		8	$4\cdot10^{-3}$	680
p+p	100	5	$1\cdot10^{-4}$	430
		8	$5.5\cdot10^{-6}$	22

Table 2: Online selection by high $\mathrm{p}_\perp$ π^0 trigger in EMC: events per GeV bin at a given $\mathrm{p}_\perp$ per day. Assumptions and details of calculation given in text.

We calculate the transverse density distribution of the reaction volume as a function of impact parameter, utilizing four different weighting functions:

- Wounded Nucleons: The transverse density profile is calculated using a Woods-Saxon density distribution and Eq. 4, appropriate for the bulk of particle production. We use σ_{NN}=30 mb, but also investigate the sensitivity of the computed quantities to this parameter.
- Binary Collisions: The transverse density profile is calculated using a Woods-Saxon density distribution and Eq. 5, appropriate for hard processes such as jet and J/Ψ production.
- Hard Sphere: The transverse density profile is calculated for colliding sharp-edged spheres, with the density defined as $\mathrm{T_A}$+$\mathrm{T_B}$. This corresponds to the limit of the Wounded Nucleon density in which the Woods-Saxon parameter a in Eq. 2 is small and σ_{NN} in Eq. 4 is large. The radius of the hard sphere corresponding to a Au nucleus is 7.24 fm, increased from the Woods-Saxon value of 6.52 fm in order to obtain the same total cross section.
- Two Dimensional: The transverse density profile is simply the area of overlap region in Fig. 1, with uniform weighting (i.e. without taking into account the nuclear thickness in the z-direction). The radius corresponding to a Au nucleus is 7.24 fm, as in the Hard Sphere calculation.

We first present the transverse density profiles graphically, and then calculate moments to compare the distributions quantitatively. Figures 3 to 6 show the transverse density profiles for Au+Au collisions as linear contour plots in one quandrant of the coordinate system defined in Fig. 1, for the four weighting functions at different impact parameters. The Wounded Nucleon and Binary Collision profiles are very similar in shape, with the Binary Collision distribution falling off slightly faster from the origin. Neither could properly be labelled “almond-shaped”, a common characterization of the

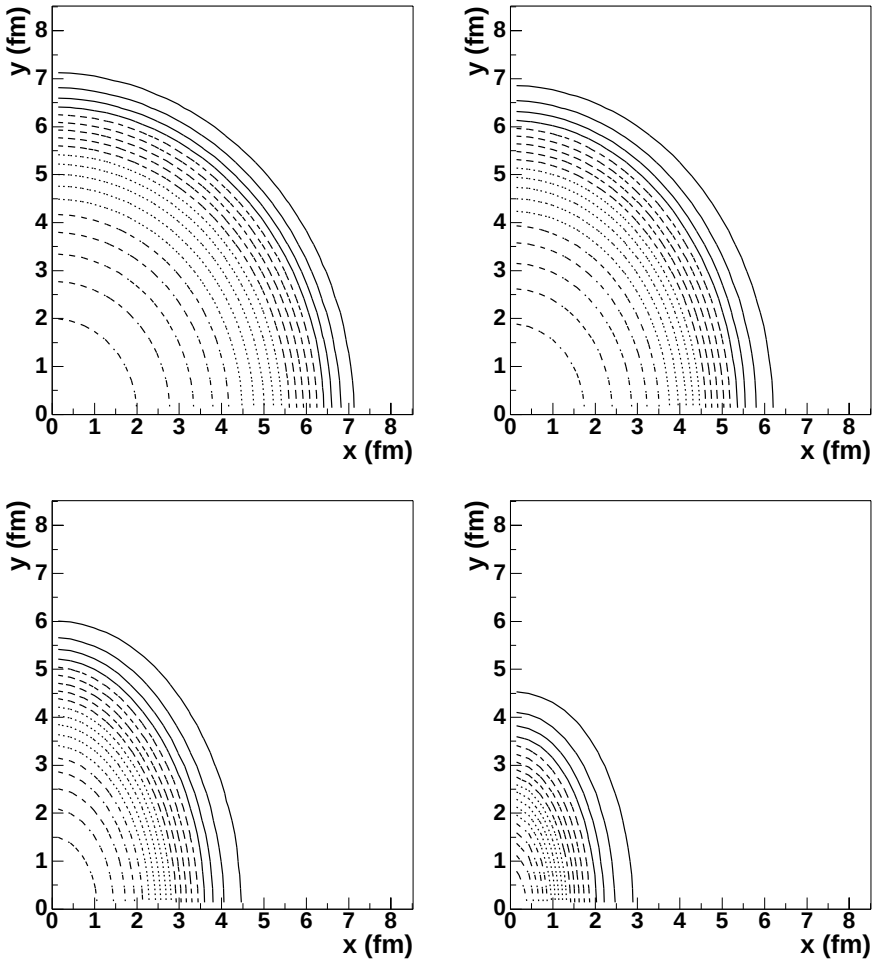

Figure 3: Transverse density of Wounded Nucleons as a function of (x,y) (see Fig 1), for collisions of Au+Au at impact parameters b=0, 4, 8 and 12 fm.

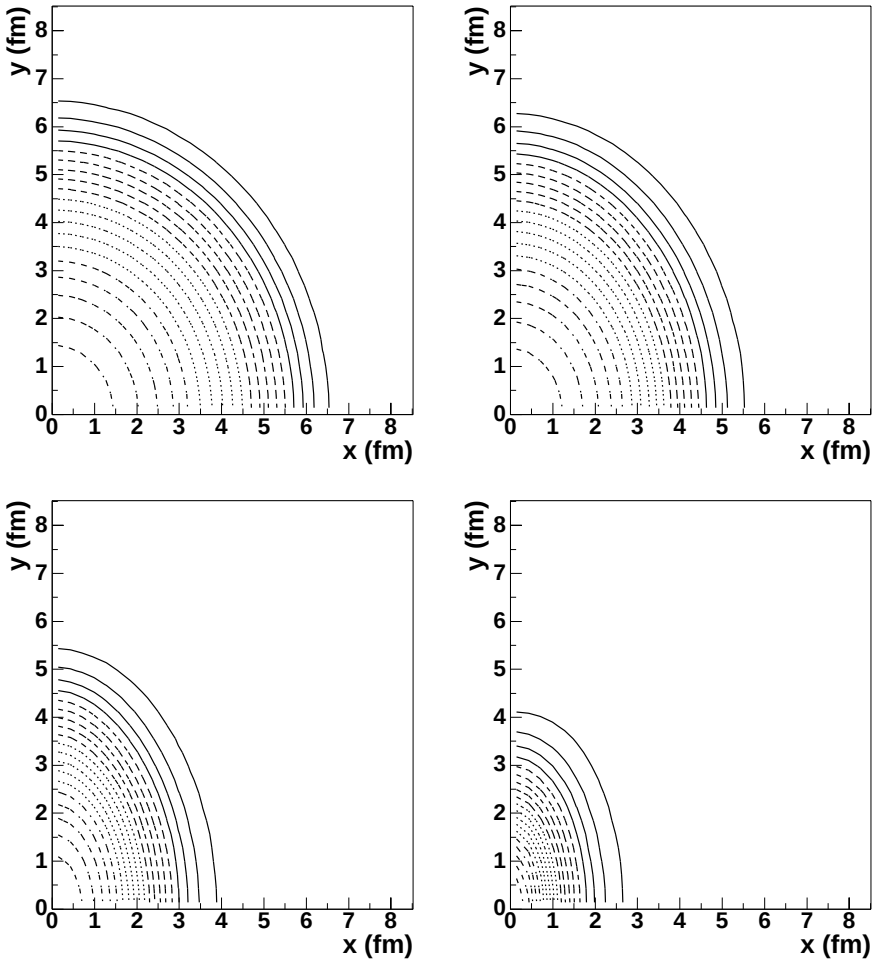

Figure 4: Transverse density of Binary Collisions as a function of (x,y) (see Fig 1), for collisions of Au+Au at impact parameters b=0, 4, 8 and 12 fm.

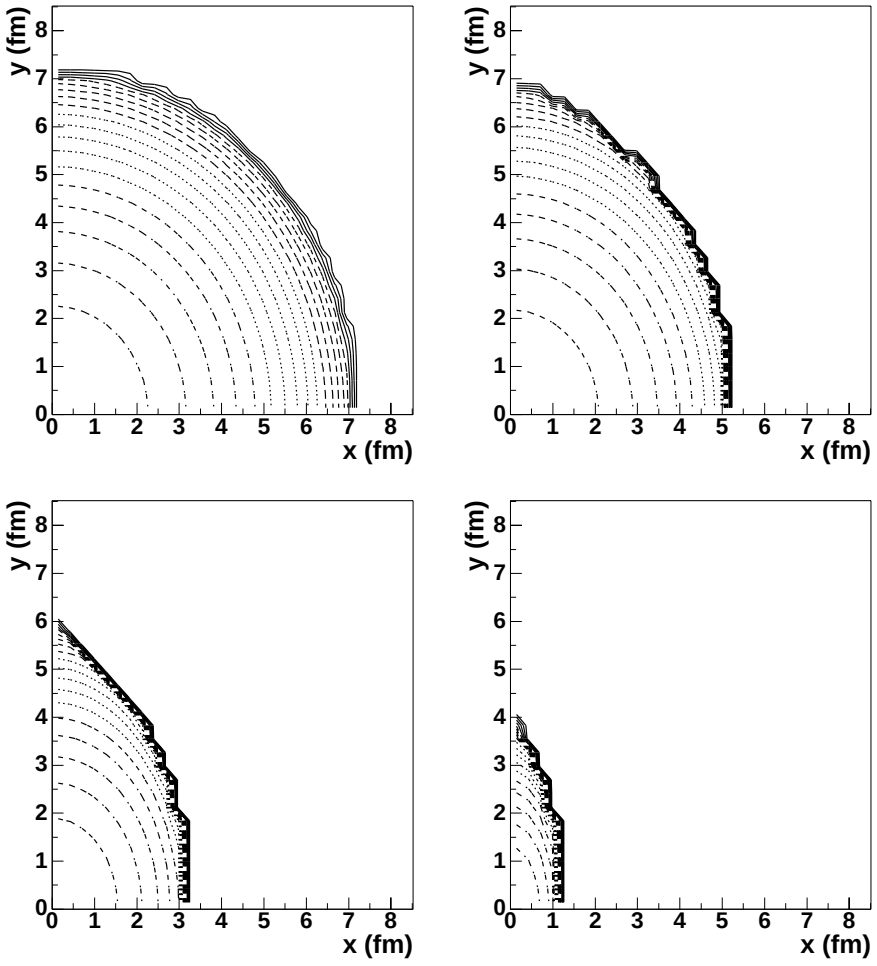

Figure 5: Transverse density profile of interacting hard spheres as a function of (x,y) (see Fig 1), corresponding to Au+Au at impact parameters b=0, 4, 8 and 12 fm.

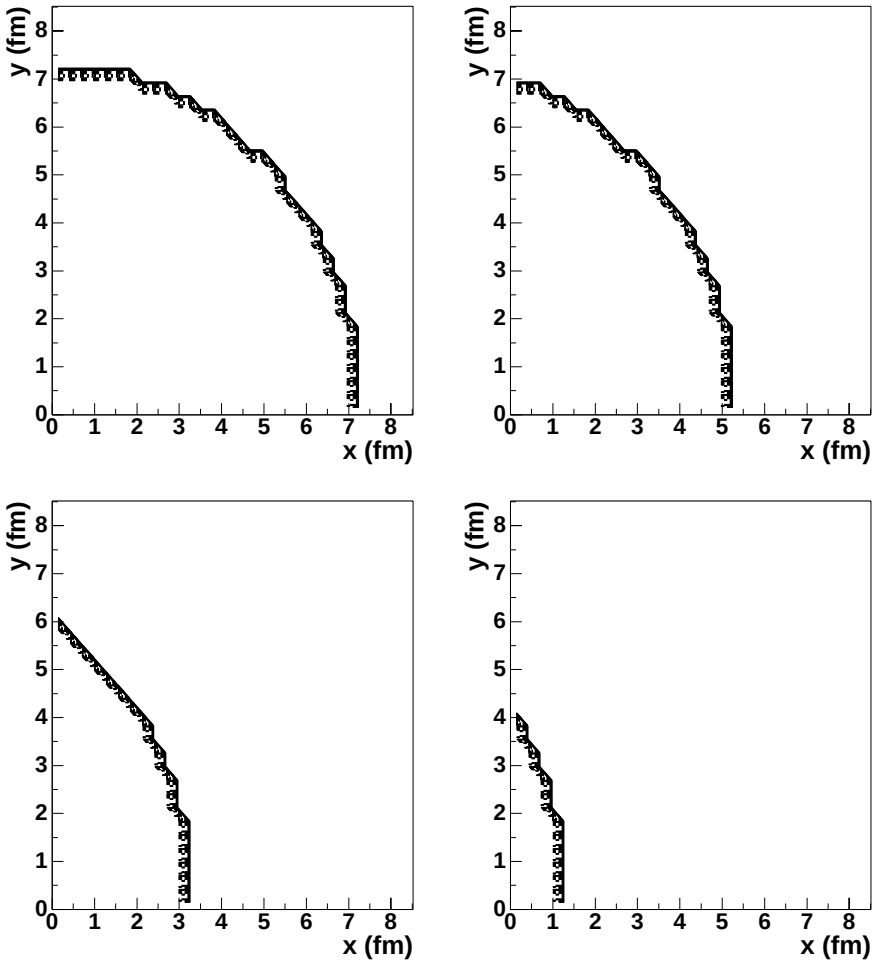

Figure 6: Two dimensional transverse density profile as a function of (x,y) (see Fig 1) corresponding to the region of overlap in Fig 1, for Au+Au collisions at impact parameters b=0, 4, 8 and 12 fm.

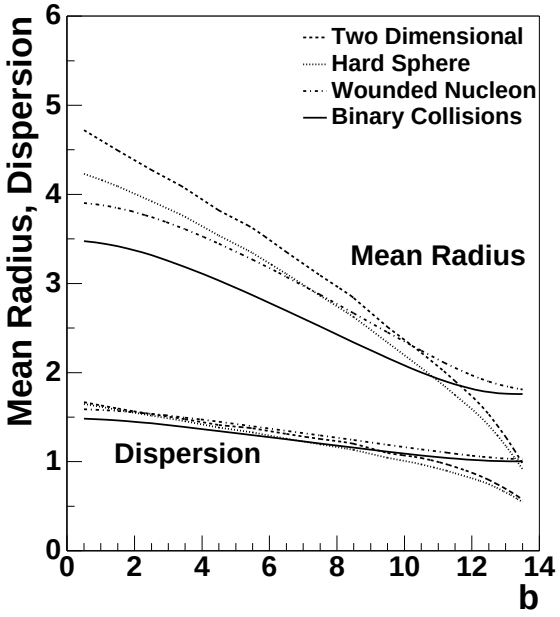

Figure 7: Mean and dispersion of radius of the interaction region as a function of impact parameter for Au+Au collisions, for the four weighting functions. The units of both axes are fm.

shape of the reaction volume for non-central collisions. The less realistic Hard Sphere and Two Dimensional calculations exhibit larger aspect ratios for noncentral collisions and unphysical sharp declines in the density at the boundaries of the overlap region, and can reasonably be labelled "almond" or "canoe-shaped".

Figure 7 shows the mean transverse radius ($<\mathrm{s}>$ in Fig. 1) and its dispersion ($\sqrt{<\mathrm{s}^2> - <\mathrm{s}>^2}$) for the four weighting functions, as a function of impact parameter for Au+Au collisions. As is seen in the density profiles themselves, the Two Dimensional and Hard Sphere functions give larger mean radii than the Wounded Nucleon and Binary Collision functions. The dispersion in the radius is similar for all four functions, and is a weak function of impact parameter. The values at large impact parameter are dominated by the treatment of the nuclear surface.

Note that in the case of Binary Collision weighting, the mean (and median) radius is about 3.5 fm for the most central collisions. In other words, about one half of all produced J/Ψ or jets are generated farther than 3.5 fm. in the transverse plane from the center of the reaction zone in central collisions, with a distribution in radius which has a half-width of about 1.5 fm. Rather few of the J/Ψ or jets are produced near the center of the reaction, due simply to the geometry of nucleus-nucleus collisions.

Figure 8 shows the eccentricity (Eq. 15) of the interaction region as a function of impact parameter for Au+Au collisions, for the four weighting functions. Also shown is the approximation b/($2\mathrm{R_A}$) from Eq. 15. The eccentricity of the Wounded Nucleon

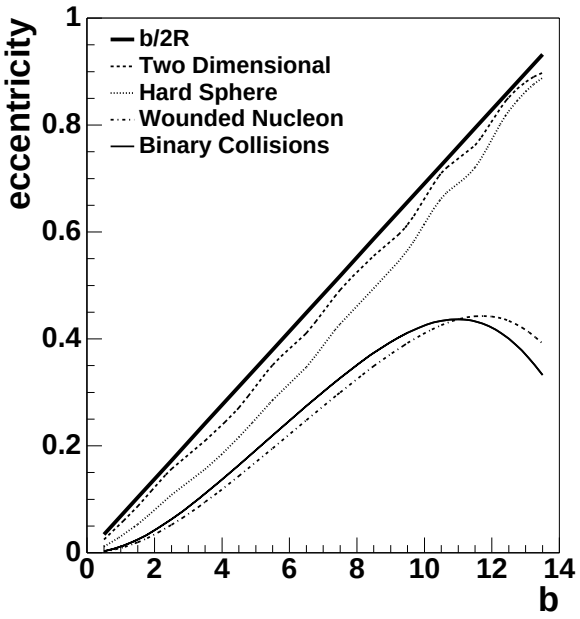

Figure 8: Eccentricity (Eq. 15) of the interaction region as a function of impact parameter for Au+Au collisions, for the four weighting functions.

and Binary Collision models are similar and significantly smaller than those of the other models. Parametrization of ϵ in the Wounded Nucleon Model and its dependence upon $\sigma_{\rm NN}$ is discussed in Appendix A.

To summarize the main results of this section:

- Within a baseline physics picture, in which the collision of heavy nuclei is simply the convolution of elementary hadronic collisions, the spatial distribution of wounded nucleons and binary collisions for small cross sections is very similar at all nuclear impact parameters.
- For central collisions of heavy nuclei, the bulk of hard scattering lies in an annulus in the transverse plane of radius $\approx\ 3.5 \pm 1.5$ fm.

5 Number of Participants and Binary Collisions

The distributions in Figures 3 to 5 can be integrated to calculate the total number of nucleon participants or binary collisions per nuclear collision as a function of nuclear impact parameter. These are presented in Tables 3 and 4 for Au+Au and Pb+Pb collisions. Columns 2 and 3 give the number of Wounded Nucleons (Equation 4) with $\sigma_{\rm NN}$=30 and 40 mb. Column 4 gives the fraction of volume of the Hard Spheres that interact, normalized to the total number of incoming nucleons. Column 5 gives the

number of binary collisions for an interaction cross section of 1 $\mu\mathrm{barn}$ (the rate for other small cross sections is obtained by linear scaling of this number).

b (fm)	# part (WN, σ_{NN}=30 mb)	# part (WN, σ_{NN}=40 mb)	# part (HS)	# BC ($\mu\mathrm{barn}^{-1}$)
0.5	368	376	389	$2.8 \cdot 10^{-2}$
1.5	355	364	366	$2.7 \cdot 10^{-2}$
2.5	331	341	335	$2.5 \cdot 10^{-2}$
3.5	298	310	302	$2.2 \cdot 10^{-2}$
4.5	262	274	263	$1.8 \cdot 10^{-2}$
5.5	223	234	226	$1.5 \cdot 10^{-2}$
6.5	183	193	187	$1.2 \cdot 10^{-2}$
7.5	144	155	148	$8.5 \cdot 10^{-3}$
8.5	108	117	115	$5.8 \cdot 10^{-3}$
9.5	77	84	82	$3.7 \cdot 10^{-3}$
10.5	49	55	54	$2.1 \cdot 10^{-3}$
11.5	28	32	32	$1.0 \cdot 10^{-3}$
12.5	13	16	15	$4.0 \cdot 10^{-4}$
13.5	5	6	4	$1.3 \cdot 10^{-4}$

Table 3: Impact parameter dependence for Au+Au collisions of the number per nuclear collision of nucleon participants in the Wounded Nucleon model (columns 2 and 3) and colliding Hard Spheres (column 4), and the number of binary scatterings with cross section 1 μbarn (column 5).

Tables 3 and 4 show only a weak dependence of the number of participants on σ_{NN}, and good agreement between the number of participants calculated with the Hard Sphere and Wounded Nucleon models. The latter point is in sharp contrast to the strong difference seen between the models for ϵ (Figure 8), and is due to the fact that the number of participants is dominated by the bulk volume, whereas ϵ is dominated by the surface overlap.

6 Radial Distribution of Hard Processes

We conclude with a discussion of the transverse density distribution of hard processes (binary collisions) with respect to the center of one of the nuclei. Refering to Fig. 1, we examine the density of binary collisions as a function of $\mathrm{b_A}$ rather than as a function of $\vec{\mathrm{s}}$ as was done in the previous sections. The distribution of hard scattering in $\mathrm{b_A}$ is relevant to the study initial state effects, such as the Cronin effect and the spatial variation of nuclear structure functions [8].

Figure 9 shows the normalized probability distribution for hard processes as a function of $\mathrm{b_A}$ for Au+Au collisions within restricted ranges of impact parameter, and for

b (fm)	# part (WN, $\sigma_{\rm NN}$=30 mb)	# part (WN, $\sigma_{\rm NN}$=40 mb)	# part (HS)	# BC (μbarn^{-1})
0.5	388	397	410	$3.0 \cdot 10^{-2}$
1.5	375	385	388	$2.9 \cdot 10^{-2}$
2.5	351	362	358	$2.6 \cdot 10^{-2}$
3.5	318	330	322	$2.3 \cdot 10^{-2}$
4.5	281	293	286	$2.0 \cdot 10^{-2}$
5.5	241	252	246	$1.6 \cdot 10^{-2}$
6.5	199	211	206	$1.3 \cdot 10^{-2}$
7.5	159	170	169	$9.5 \cdot 10^{-3}$
8.5	121	131	132	$6.7 \cdot 10^{-3}$
9.5	87	95	99	$4.3 \cdot 10^{-3}$
10.5	58	64	69	$2.5 \cdot 10^{-3}$
11.5	34	39	44	$1.3 \cdot 10^{-3}$
12.5	17	20	23	$5.5 \cdot 10^{-4}$
13.5	7	9	8	$1.9 \cdot 10^{-4}$

Table 4: Impact parameter dependence for Pb+Pb collisions of the number per nuclear collision of nucleon participants in the Wounded Nucleon model (columns 2 and 3) and colliding Hard Spheres (column 4), and the number of binary scatterings with cross section 1 μbarn (column 5).

p+Au collisions triggered on a hard process with no additional event charaterization[3]. As in the previous sections, we see that the bulk of the production occurs well away from the center of the nucleus for all impact parameters. The distributions for impact parameters in the range $0 < \mathrm{b} < 6$ fm are very similar. As the impact parameter increases, the distribution becomes confined to the nuclear surface.

For the p+Au case, the distribution is plotted relative to the origin of the Au nucleus. The distribution for inelastic p+Au collisions increases linearly from the origin to about 7.5 fm (not shown for clarity). Since all distributions are normalized, the inelastic distribution would lie below the hard scattering one in this region, so that triggering on a hard process in p+Au collisions biases the event selection towards more central events.

It is interesting to note that the p+Au and central Au+Au distributions in Fig. 9 are quite similar. This may aid in connecting the initial state effects observed in p+Au collisions to their contributions in central collisions of heavy nuclei.

[3]Characterizing the centrality of a very light nucleus colliding with a heavy one may be achievable at RHIC by measuring the total multiplicity for $\mathrm{p}_\perp < 1$ GeV in a wide rapidity range. This technique appears not to have sufficient resolution for p+Au collisions, but may do so for Li+Au.

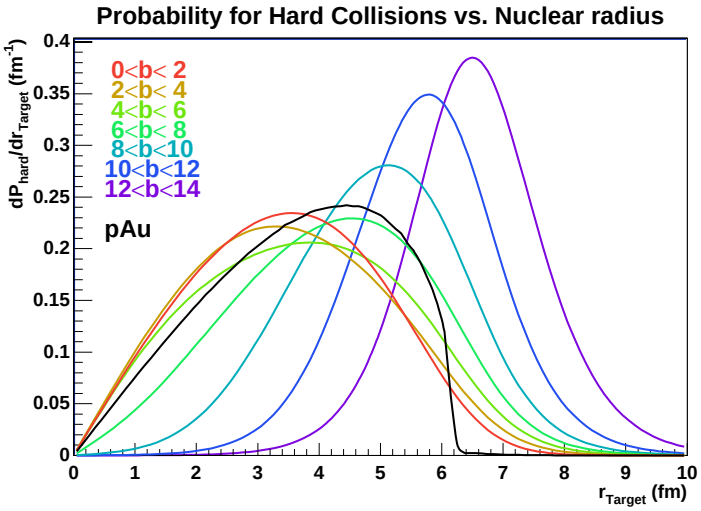

Figure 9: Normalized probability distribution of hard processes as a function of the distance to the center of one of the colliding nuclei ($\mathrm{b_A}$ in Fig. 1), for Au+Au collisions within a range of impact parameters and for p+Au collisions tiggered solely on a hard process.

7 Acknowledgements

We thank Art Poskanzer, Raimond Snellings, Thomas Ullrich, Ramona Vogt, and Sergei Voloshin for valuable discussions.

A ϵ and S in the Wounded Nucleon Model

In this appendix we give a more detailed discussion of the characterization of the geometry of the interaction region in the Wounded Nucleon Model. The elliptic anisotropy of the overlap region ϵ, defined in Eq. 15, is shown as a function of impact parameter in Fig. 8 for all four models for Au+Au collisions. ϵ is parametrized for the Wounded Nucleon Model (σ_{NN}=30 mb) as

$$\epsilon(\mathrm{b}) = -0.0469x + 2.754x^2 - 4.797x^3 + 4.852x^4 - 2.492x^5 \qquad (16)$$

where $x = \mathrm{b}/(2\mathrm{R})$ and $2\mathrm{R} = 15$ fm. for Pb+Pb collisions and $2\mathrm{R} = 14.7$ fm. for Au+Au collisions.

Increase of σ_{NN} to 40 mb decreases ϵ by 13% at b=2.5 fm and 4% at b=10.5 fm, with the change monotonic in b. The decrease of ϵ with increasing σ_{NN} can be understood by noting that the value of ϵ is dominated by surface effects. Increasing σ_{NN} effectively extends the surface to larger radii, with the consequence that the shape of the interaction region in the transverse projection is less eccentric than for σ_{NN}=30 mb at the same impact parameter.

For reference, we also include a parametrization in the same model of the impact parameter dependence of the quantity $S = \pi R_x R_y$ [13]. Here, $R_x = \sqrt{< x^2 >}$, $R_y = \sqrt{< y^2 >}$, and $< \ldots >$ denotes the spatial average used in Equation 15. In [13], S is used to calculate the particle density in the overlap region. The parametrization is

$$S(\mathrm{b})/(\pi \mathrm{R}^2) = 0.164 + 0.0141x - 0.684x^2 + 1.026x^3 - 0.763x^4 + 0.284x^5 \quad (17)$$

where, again, $x = \mathrm{b}/(2\mathrm{R})$ and $2\mathrm{R} = 15$ fm. for Pb+Pb collisions and $2\mathrm{R} = 14.7$ fm. for Au+Au collisions.

References

[1] W. Busza and R. Ledoux, Ann. Rev. Nucl. Part. Sci. **38**, 119 (1988).

[2] H. Appelshäuser et al. (NA49 Collaboration), Phys. Rev. Lett. **82**, 2471 (1999).

[3] K. J. Eskola, K. Kajante and J. Lindfors, Nucl. Phys. **B323**, 37 (1989).

[4] R.J. Glauber and G. Matthiae, Nucl. Phys. **B21**, 135 (1970); J. Hüfner and J. Knoll, Nucl. Phys. **A290**, 460 (1977); R. W. Hasse and W. D Meyers, "Geometrical Relationships of Macroscopic Nuclear Physics", Springer Series in Nuclear and Particle Physics, Springer-Verlag, 1988.

[5] R. Vogt, nucl-th/9903051.

[6] D. M. Alde *et al.* (E772 Collaboration), Phys. Rev. Lett. **66**, 133 (1991).

[7] X.N. Wang, nucl-th/9711026, Fig. 1.

[8] V. Emel'yanov, A. Khodinov, S. R. Klein and R. Vogt, Phys. Rev. **C56**, 2726 (1997); Phys. Rev. Lett. **81**, 1801 (1998).

[9] R.J.M. Snellings, A.M. Poskanzer, and S.A. Voloshin, STAR Note 388.

[10] H. Appelshäuser et al. (NA49 Collaboration), Phys. Rev. Lett. **80**, 4136 (1998).

[11] H. Heiselberg and R. Matiello, nucl-th/9901004.

[12] H. Sorge, Phys. Rev. Lett. **82**, 2048 (1999).

[13] H. Heiselberg and A.-M. Levy, Phys. Rev. **C59**, 2716 (1999).